Effects of Remaining Hair Cells on Cochlear Implant Function

12th Quarterly Progress Report

C. A. Miller, B.K. Robinson, P.J. Abbas, K.V. Nourski, F.C. Jeng

Department of Otolaryngology-Head and Neck Surgery
&
Department of Speech Pathology and Audiology

University of Iowa

Iowa City, Iowa, USA

July 27, 2005

File: N01-DC-2-1005QPR12.PDF

Effects of Remaining Hair Cells on Cochlear Implant Function
N01-DC-2-1005QPR12
Neural Prosthesis Program

Table of Contents

Effects of Remaining Hair Cells on Cochlear Implant Function
N01-DC-2-1005QPR12
Neural Prosthesis Program

1. Summary of Activities in This Quarter

During this reporting period (1 April – 30 June, 2005) we accomplished the following:

1. We performed 2 acute guinea pig experiments that extend our work on ECAP measures of acoustic and electric stimulus interactions. Specifically, we continued work (first described in QPR 10) to compare the post-adaptation effects caused by an acoustic masker to that produced by an electric masker. That work is aimed at determining whether or not our observed acoustic masking effects (on the ECAP) are unique to the acoustic stimulus or merely related to neural activity, irrespective of the method of excitation.

2. We performed 3 acute guinea pig experiments recording multi-unit responses from the inferior colliculus in response to combined acoustic and electric stimulation.

3. We performed four acute cat experiments. Three of these preparations yielded significant sets of single-fiber data, while all four yielded ECAP data. The focus of the single-fiber experiments has shifted from earlier sessions in that priority was given to assessing best frequency and threshold of each fiber.

4. We completed most analyses of single-fiber recordings and the associated data reduction. We note a technical detail of importance for accurate spike detection: In our experience, the application of automated stimulus artifact reduction schemes (i.e., procedures based on statistical estimates of spike and stimulus-artifact amplitudes) results in occasional failures in computing appropriate templates. This is particularly the case when computing the n templates applied to an n-pulse train of electric stimuli. Such errors are typically easy to detect in raster plots (e.g., as a "drop out" in spikes), but must be corrected manually, by user intervention in the process of selecting the template thresholds.

   Characterization of the completed single-fiber data sets are the major focus of this progress report.

5. We completed developmental work on a computational model (implemented using Matlab) to simulate refractory and adaptation effects in acoustically stimulated auditory nerve fibers (ANF's). The model follows the approach of Schroeder & Hall (1974). Work continues on adapting the model to account for combined acoustic and electric stimulation in order to use it to test our hypotheses of interaction effects that we have observed in our ECAP measures (Nourski et al., 2005).

2. Focus topic: Single-fiber measures of electric responses in acoustically sensitive ears

2.1   Introduction

Work conducted under this contract examines the responses of the auditory system to combined electric and acoustic stimulation using animal models of implanted ears with residual acoustic sensitivity. This work includes measures of auditory nerve responses (single-fiber and whole-nerve potentials) and multi-unit activity within the inferior colliculus. Measures of single auditory nerve fiber responses serve two functions: to reveal basic response properties under hybrid (acoustic-electric) stimulation and to provide a means of interpreting the electrically evoked compound action potential, a response that can be routinely obtained from many cochlear implant users.

In this report, we focus on single auditory nerve fiber responses obtained from acute cat preparations implanted with a minimally invasive intracochlear stimulating electrode, as has been described in previous reports. Our stimulus paradigm consists of the interleaved presentation of (1) a moderate-rate (250 pps) electric pulse train, (2) a wideband acoustic noise burst (duration 100-400 ms), and (3) both stimuli presented simultaneously, as has been described previously. In all cases when the two stimuli are presented together, the noise burst is preceded by 50 ms of electric (alone) pulses and followed by 100-200 ms of electric (alone) pulses to establish baseline firing characteristics and fiber recovery characteristics following offset of the acoustic noise. To assess ANF firing properties, we typically use 30-40 repeated presentations of each of the three types of stimuli.

We have hypothesized several ways in which electric and acoustic stimuli could interact at the cochlear level, based upon previously published observations of electrically evoked ANF responses modulated either by the presence of functional hair cells or acoustically evoked activity. It is not surprising, therefore, that the ANF response patterns observed to date are more complex than those typically reported from electrically stimulated nerves of deafened cochleae. Thus, the report characterizes ANF responses as a group, in an attempt to describe overall patterns and also presents individual fiber data for responses that are not uniformly observed across all fibers.

Our last report of ANF responses reported on a modest data set (10 fibers). In this report, we summarize larger sets of single-fiber data collected to date. For inclusion in this report, each cat preparation had to exhibit a significant amount of residual hearing, as assessed by click-evoked CAP. Cats with shifts greater than 40 dB were excluded. In our more recent experiments, we have emphasized collecting acoustic "best frequency" data at the expense of more detailed data sets on electric-acoustic interactions.

Details of the methods and stimulus protocols have been described in previous reports and are unchanged from those reports unless specifically noted otherwise.

2.2   General fiber characteristics

Figure 1 summarizes the subset of fibers from which we obtained acoustic frequency tuning data. Pure-tone thresholds are plotted versus best frequency, along with the contour line of mean thresholds for high spontaneous rate fibers reported by Liberman and Kiang (1978). The mean cochlear location of our stimulating electrode (15-16 kHz place) is shown at the lower right corner of the graph. It was estimated from our collection of dissected cochleae and the frequency-place map of Liberman (1982). The various symbol types indicate high and low spontaneous rates (using a 25 spike/s criterion rate) and the confirmed presence of electrophonic activity. Our data indicate that acoustic tuning and sensitivity can be maintained in our preparations; however, some loss of sensitivity (about 20-30 dB) is evident in most cases. The data also suggest the possibility of somewhat greater loss (or variability) at high frequencies near the place of electrode insertion.

In our earlier cats, acoustic levels were often not sufficiently explored to estimate threshold; in those cases, best frequency is shown using a downward-pointing arrowhead to indicate the lowest level assessed. The shapes of the remaining symbols indicate fibers with low (<25 spike/s) spontaneous rates (downward triangles), high (>25 spike/s) spontaneous rates (upward triangles), and fibers where spontaneous rate was not determined (circles). Thresholds from our animals are somewhat higher than those reported by Liberman, suggesting that the cochleostomy and electrode insertion results in some loss. Also, the data suggest that acoustic sensitivity shifts are greater at the base, near the site of the electrode.

Fibers from which electrophonic (beta) responses were clearly evident are indicated by symbols incorporating "+" symbols. Across 130 surveyed fibers, we observed clear evidence of electrophonic responses in 27 cases for an incidence rate of 21%. This is higher than the 6% incidence reported by van den Honert & Stypulkowski (1984) for intracochlear stimulation and comparable to their rate (19%) for extracochlear stimulation.

Figure 2 shows a spontaneous-rate (SR) histogram based on 99 fibers from which SR measures were obtained. Using a low-rate / high-rate cutoff criterion of 25 spike/s, 45% of the fibers were categorized as low SR and 55% were high SR fibers. This can be compared against the 39% / 61% ratio reported in cats raised in low-noise chambers, which typically have a greater fraction of "high spont" fibers than do "normal" cats obtained from animal vendors (Liberman 1978). Thus, with the somewhat limited sample reported here, our distribution of high and low SR fibers is within expectations of "normal" cats. In a sample of 56 fibers from which spontaneous rate and electrophonic (presence / absence) assessments were made, 5 of the 20 low SR fiber (25%) demonstrated a beta response, while 17 of 36 high SR (47%) fibers showed a beta response, suggesting a bias toward more electrophonic activity in high SR fibers.
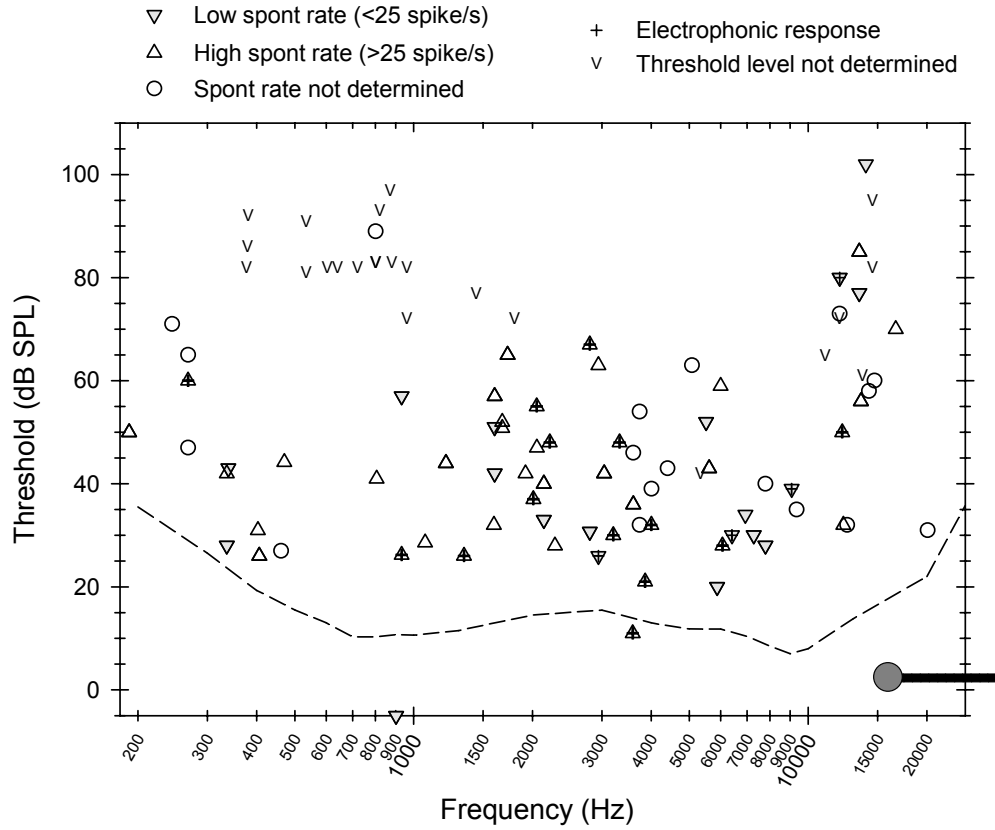
Figure 1 Threshold vs. best frequency for ANF's from cat preparations in which a monopolar intracochlear electrode was inserted into the basal turn of the cochlea. In the earlier experiments, insufficient data were collected to determine threshold ("V" symbols). The line plot indicates the mean threshold of high SR fibers measured from the "control" cats of Liberman and Kiang (1978)
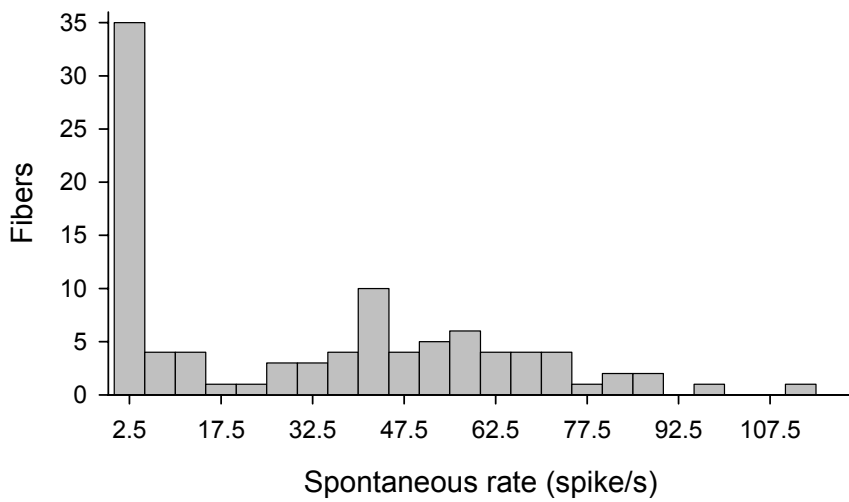
Figure 2 Histogram of the spontaneous rates of 99 fibers examined in this report. The criterion for separating low SR and high SR fibers was chosen to be 25 spike/s.
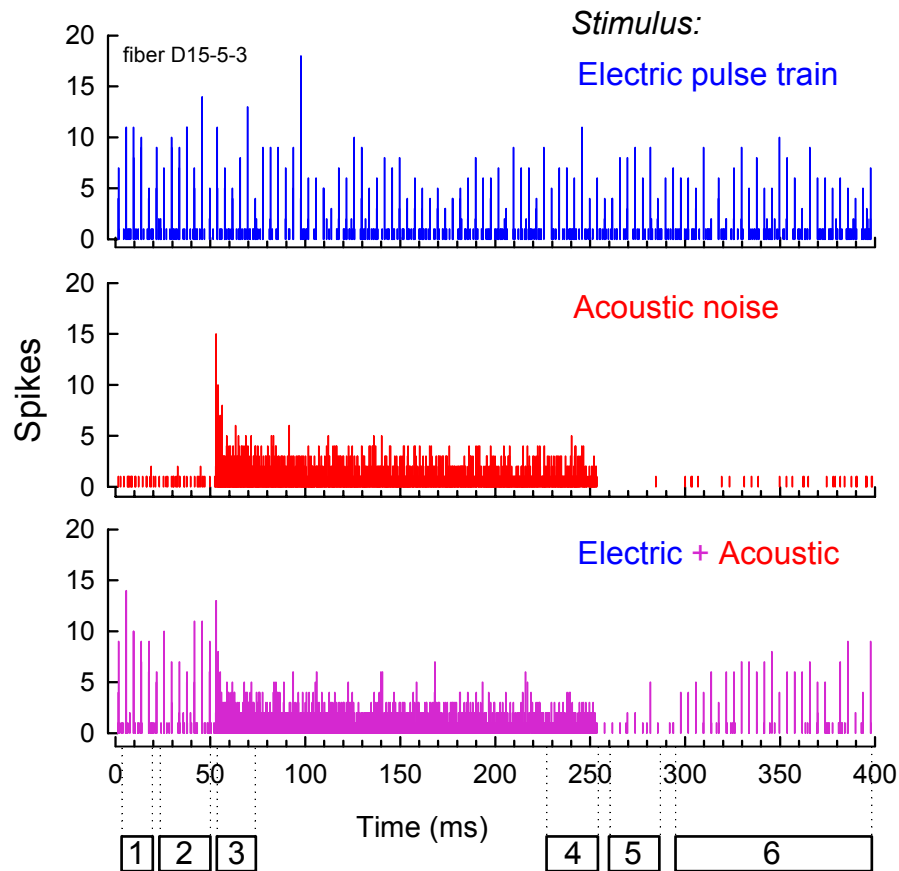
Figure 3 Examples of PST histograms collected under the hybrid (acoustic and electric) stimulus protocol used in our experiments. The electric stimulus consists of a 250 pps train of 40 μs/phase biphasic pulses. The acoustic stimulus is a wideband acoustic noise burst; in the example shown here, its duration is 200 ms. To reduce the data sets in order to characterize fiber responses across fibers, six analysis intervals, as shown, were defined. Firing statistics (rate or probability, jitter, VS, and amplitude) were computed and expressed as single mean values for each analysis interval.

In this section, we examine the response properties of a population of 41 single fibers considered as a group. As in our previous reports, were have characterized single-fiber acoustic/electric interactions as a group by considering six response epochs defined relative to the onset and offset times of the electric and acoustic stimuli. This analysis scheme is depicted in Figure 3. Note, for example, that effects related to the onset of the wide-band acoustic noise are obtained by analysis of fiber responses in interval 3, while the post noise offset effects are characterized by the responses within interval 5. The use of such intervals reduces the temporal precision of our measures, but provides more stable firing statistics. In all cases, a high-level (80-101 dB SPL overall level) acoustic noise burst was used.

2.3   Electrically evoked responses: temporal properties

Prior to examining the effects of combined acoustic and electric stimulation, we first examine the temporal properties of single fibers in response to the 250 pps electric train presented alone. Figure 4-A plots all jitter measures as a function of firing efficiency for the 41 fibers. Each fiber contributes several data as measures are not collapsed across stimulus level or analysis window. This scatter plot indicates a high level of temporal uncertainly – an order of magnitude greater than the range reported from deafened cochleae (Miller et al., 1999). Spontaneous activity has a strong effect on jitter. With the notable exception of the low SR fiber with observed electrophonic activity (filled triangles of Figure 4A), the low SR and high SR fibers are generally segregated by jitter.

Figure 4-B examines this dependency in greater detail. In this plot, mean jitter values were computed across analysis intervals 3 through 6 (cf. Figure 2) so as to obtain more stable measures and avoid the transient effects of electrophonic responses (discussed below). The data were selected for firing efficiencies greater than 70%, again to obtain more stable estimates. The jitter vs. SR curve follows a simple negative exponential model; the indicated fitted curve accounts for 73% of the observed variance.

Electrophonic activity, which is presumed to be due to the electrical activation of the outer hair cell contractile mechanism, complicates the temporal response. In QPR 6, we presented a limited amount of data on this response and presented an example (Figure 10 of that report) that suggested a possible "trading relationship" between the α and β response. While a pulse train, together with the refractory state, could produce such a relationship, additional observations suggest that this is not typically the case with our stimulus. Figure 5 shows the response histograms for a fiber exhibiting both the α and β responses. As is frequently observed, the β response adapts rather quickly, reaching a low, asymptotic, value within 50 to 60 ms after onset of the pulse train. The level series shown in this figure demonstrates the well-established trend for the electrophonic response to occur at relatively low levels. In the case shown here, the β response is relatively insensitive to increases in stimulus level, even as the direct response goes from zero to a nearly saturated response. Two additional examples of electrophonic responses from another cat are shown in Figure 6. In these cases, the β response is less robust and adapts somewhat faster.
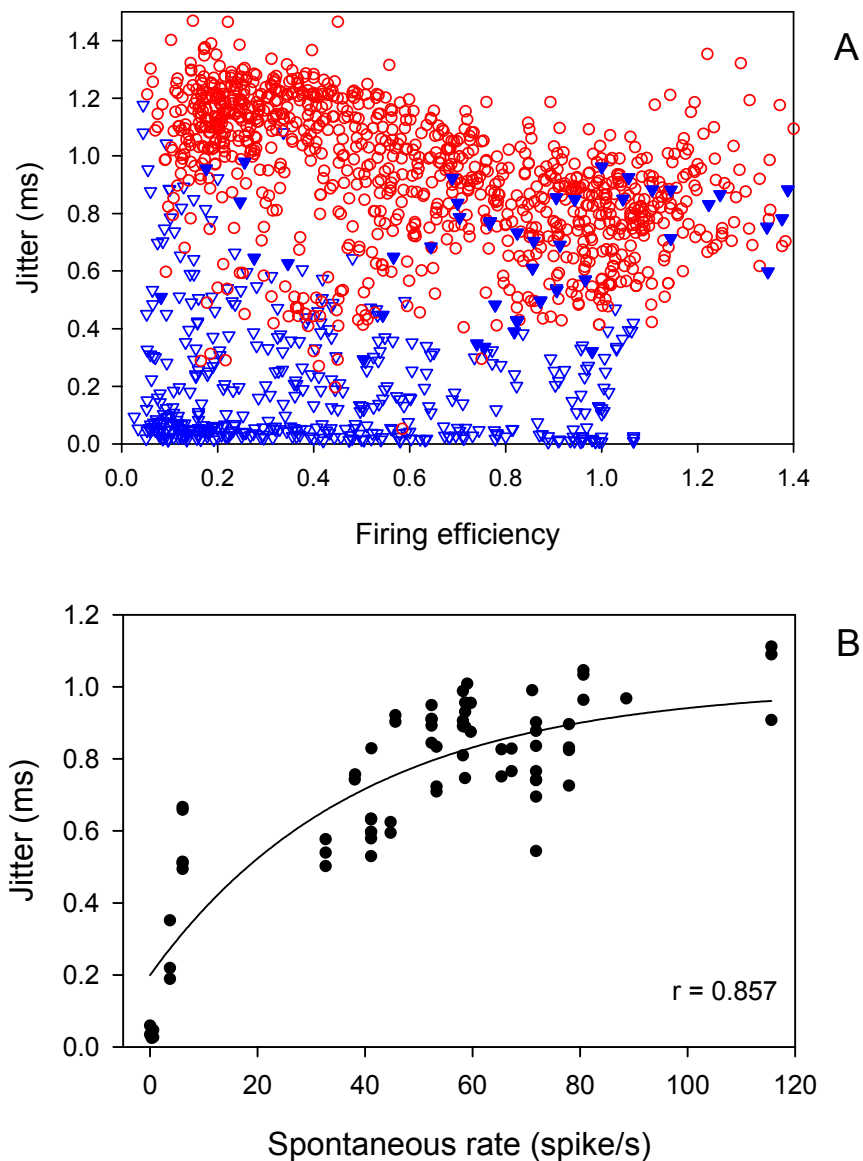
Figure 4-A   Jitter in response to electric pulses presented alone, plotted as a function of firing efficiency (probability). Circles indicate data from high SR fibers, triangles indicate low SR data, while the filled triangles indicate data obtained from a low SR fiber with an electrophonic response. Jitter measures were obtained across multiple electric levels and across all six analysis intervals. Separate analyses for each window failed to alter the basic form of the data (with the exception of some reduction in jitter in some cases through the exclusion of interval 1, which typically contained β responses, if present.

Figure 4-B   Jitter measured in response to electrical stimulation, plotted as function of each fiber's spontaneous rate. Data were selected (from the set shown in Fig 4-A) on the basis of a firing efficiency of 70% or greater. A least squared error curve fit is shown superimposed over the data.
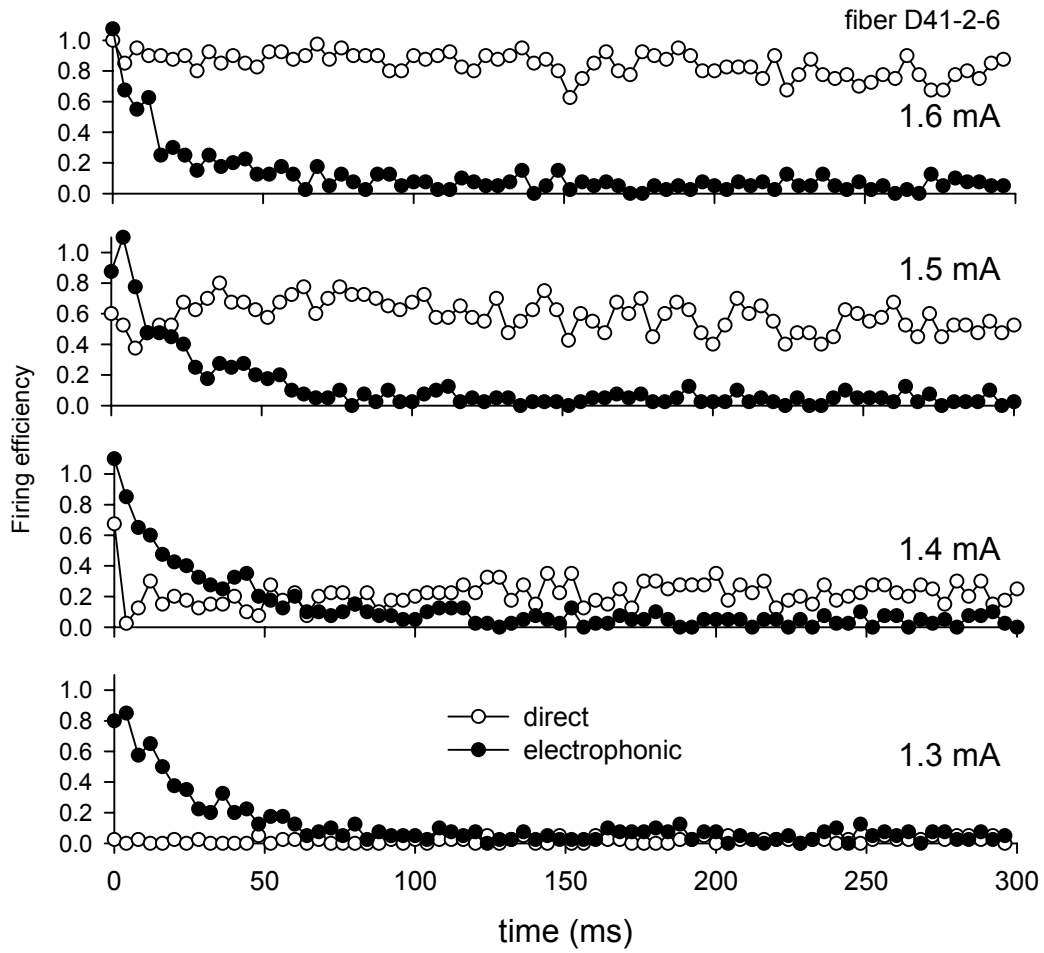
Figure 5 PSTH's of a fiber exhibiting both a direct (α) and an electrophonic (β) response. Electric stimulus level is noted in each panel. Stimulus was the same standard 250 pps electric pulse train used in all experiments. Time on the abscissa refers to the onset of the electric pulse train.
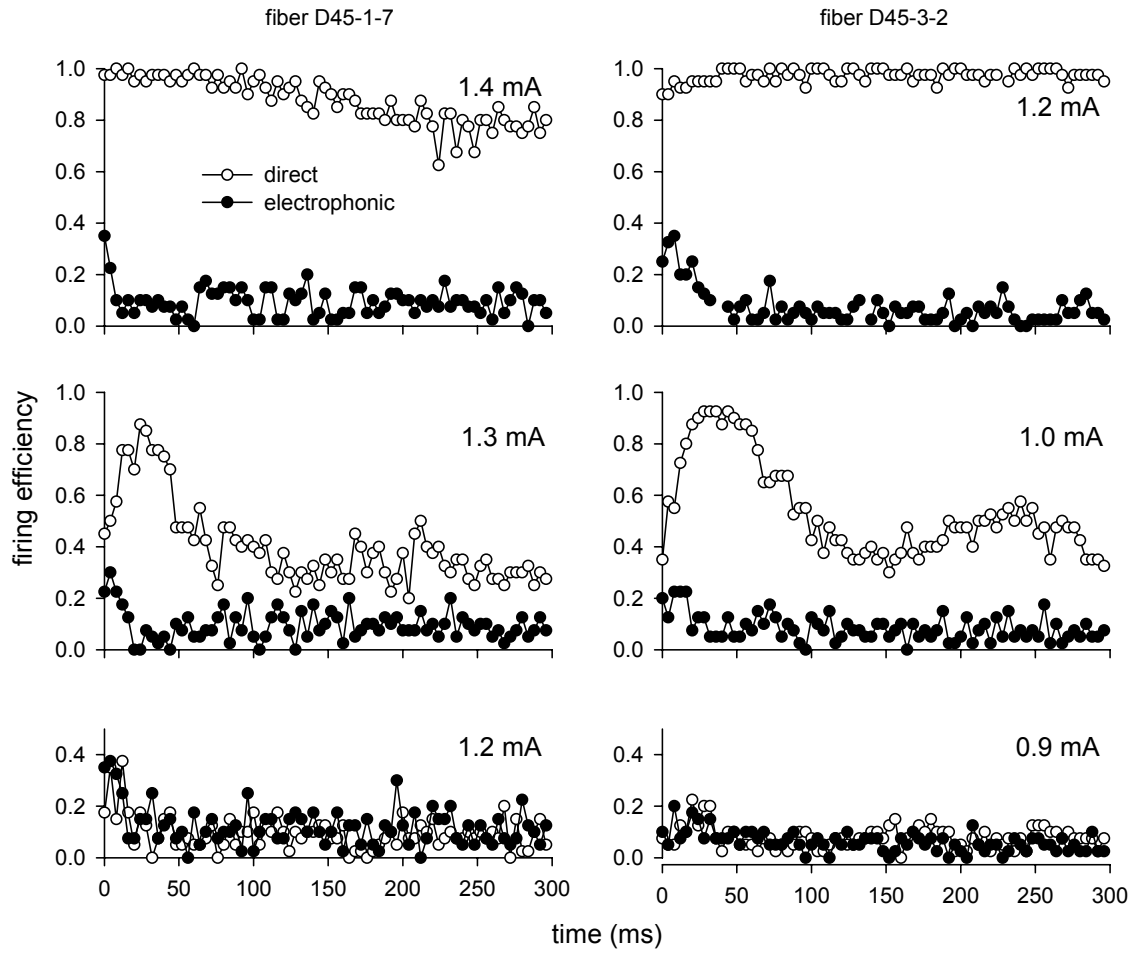
Figure 6 PSTH's from two additional fibers that exhibited both a direct and an electrophonic response. Stimulus was the same standard 250 pps electric pulse train used in all experiments.
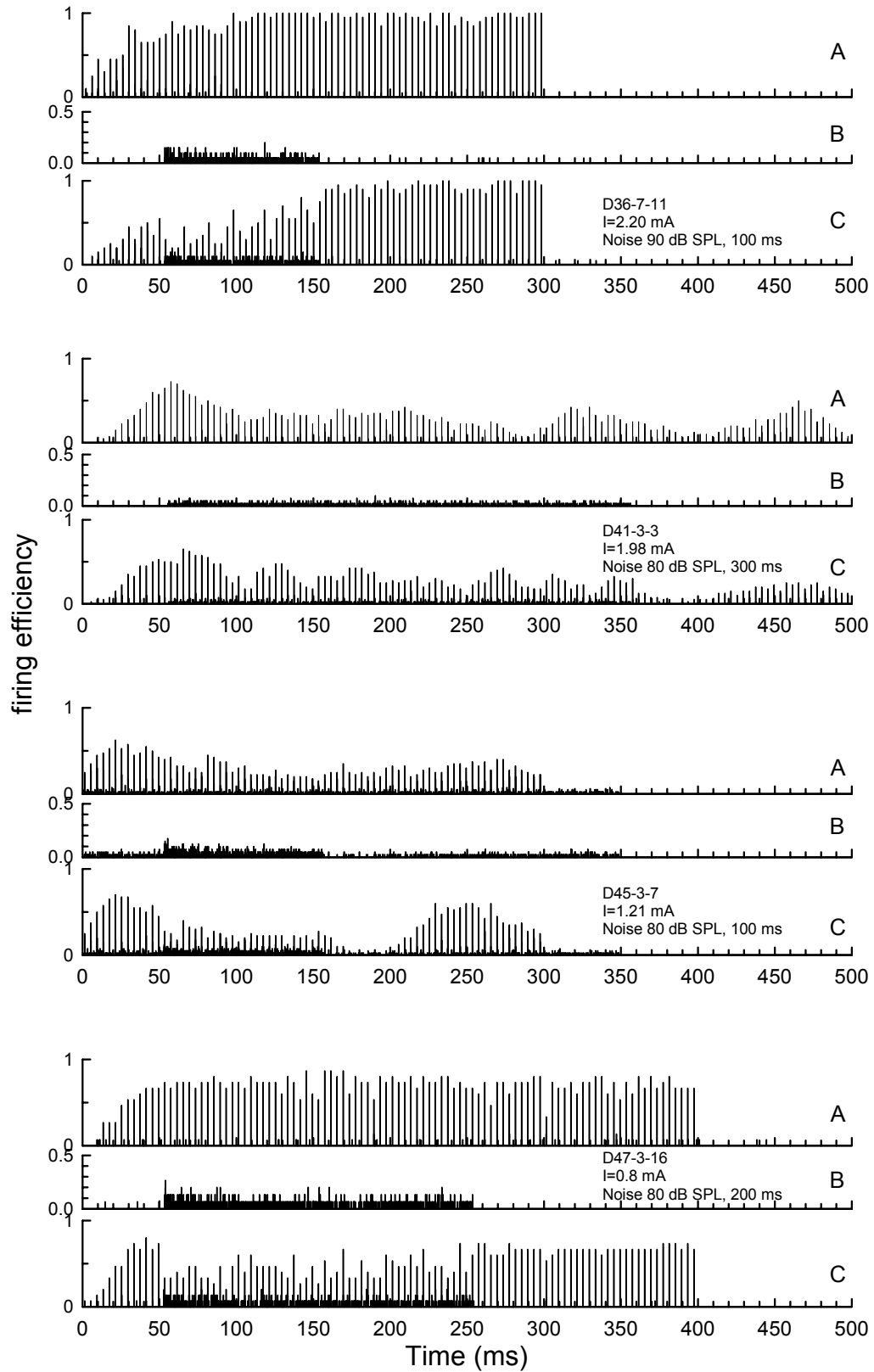
Figure 7 PSTH's from four additional fibers that demonstrate a "build-up" response to the electric pulse train. For each fiber, three panels (A, B. and C) correspond to the stimulus conditions of "electric alone", "acoustic alone" , and "electric + acoustic", respectively. Only fiber D45-3-7 exhibited an identifiable electrophonic response.

While the α and β responses of fiber D45-1-7 (left column, middle panel) demonstrate somewhat reciprocal response rates, we believe that the two opposing trends may not appear to be causally linked, at least in the straightforward manner suggested by the histograms. Rather, the "build-up" pattern observed in the α response has been observed in several fibers, across animals, regardless of the presence of a measurable electrophonic response. Examples of this build-up response are shown for four single fibers in Figure 7.

We have also observed this kind of response pattern in three of six cat experiments in which parallel ECAP measures were obtained. Figure 8 plots ECAP amplitudes in response to a 250 pps electric pulse train from a cat exhibiting this build-up response. Note that the "build up" response pattern appears at relatively high electric stimulus levels. This is a consistent observation in the animals from which these ECAP patterns have been observed to date. We are unaware of previous observations of this kind of response to electric pulse trains in deafened animals, leading us to suspect that some aspect of cochlear physiology is relevant to this modulation in fiber responsiveness.

2.4   Responses to combined electric and acoustic stimuli

As in an earlier report, were have characterized single-fiber acoustic/electric interactions as a group by considering six response epochs defined relative to the onset and offset times of the electric and acoustic stimuli, as depicted in Figure 3. Note, for example, that effects related to the onset of the wide-band acoustic noise are obtained by analysis of fiber responses in interval 3, while the post-noise offset effects are characterized by the responses within interval 5. The use of such intervals reduces the temporal precision of our measures, but provides more stable firing statistics. In all cases, a high-level (90-101 dB SPL overall level) acoustic noise burst was used and electric levels were set to produce an initial firing efficiency greater than 50%. To date, we have analyzed 41 fibers with this approach. Each fiber of this set provided an SR estimate and for 29 of the fibers, measures were obtained using both a 100 ms and a 300 ms duration acoustic noise burst. Best-frequency and threshold were measured in 19 cases.

A summary of the six-interval analyses is provided in Figure 9. As we have reported previously, measures of spike rate, jitter, and vector strength are expressed as ratios of the measures obtained during the "electric + acoustic' condition and the "electric" alone condition so as to produce measures that express the added effect of the acoustic noise on the electric pulse train. Most trends are similar to those reported previously: Firing rate and temporal uncertainty are increased during the simultaneous 'electric + acoustic" presentation during intervals 3 and 4, while firing rate and jitter are reduced in interval 5. Our larger data set now reveals a statistically significant effect (p_{error} =0.03) of acoustic duration: greater rate suppression in interval 5 is observed for the 300 ms duration noise burst. However, no additional decrement in temporal uncertainty was observed with increased noise duration.
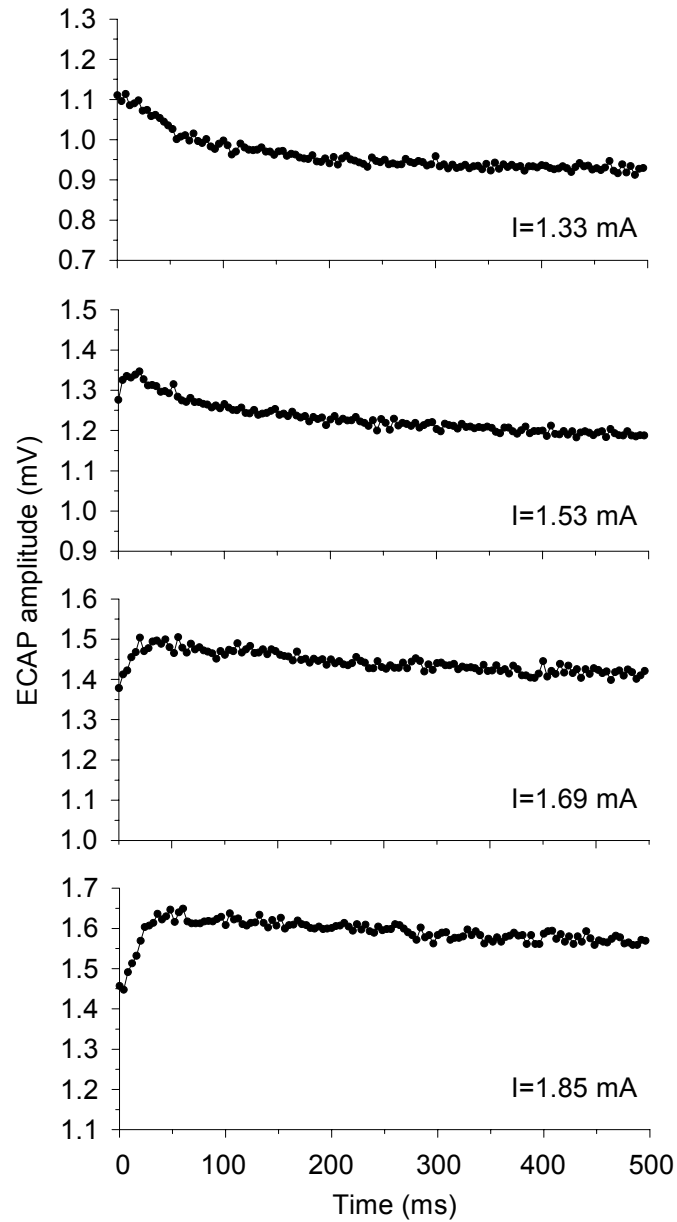
Figure 8   ECAP amplitudes obtained in response to a 250 pps electric pulse train from subject D41. The "build-up" response often observed in single-fiber responses is evident in this gross potential. Stimulus levels are noted in each panel.
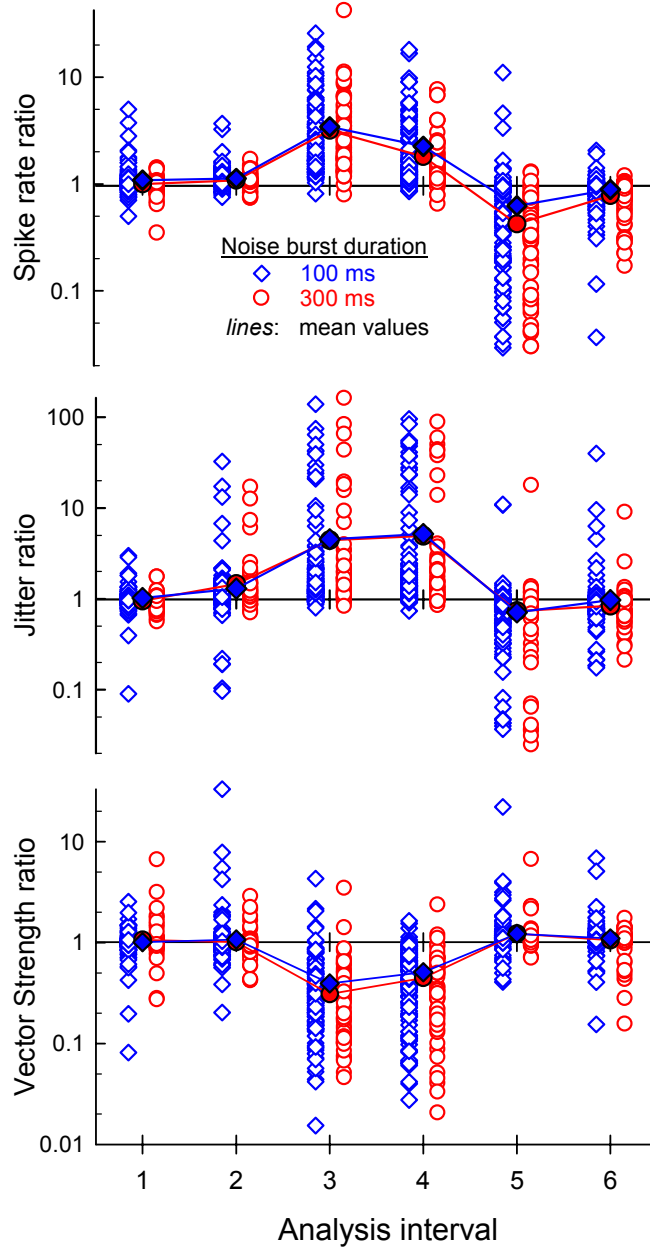
Figure 9 Summary of single-fiber responses obtained from 41 fibers of five cats. To assess the influence of the acoustic noise on the response to the electric pulse train, each of the dependent variables are computed as a ratio of the value obtained under the combined (acoustic + electric) stimuli and the electric-alone condition. The six analysis windows are those defined in Figure 3. Mean values are shown by solid symbols connected by line segments.
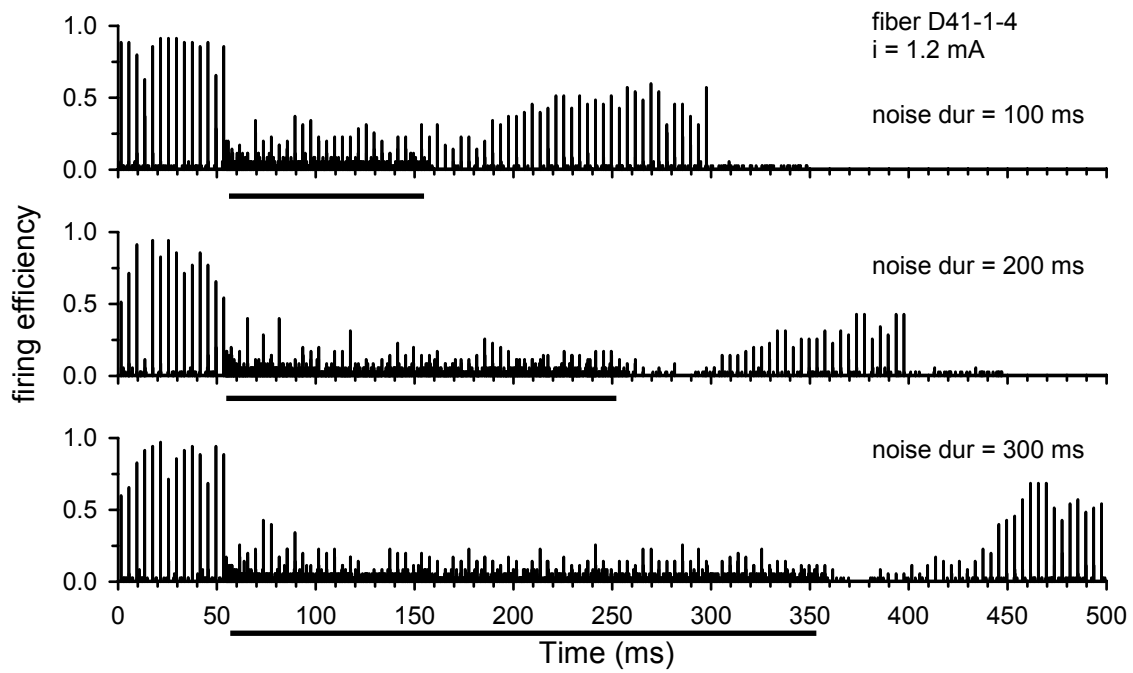
Figure 10 PSTH's from a fiber in response to combined electric and acoustic stimulation. The effects of the duration of the acoustic noise are evident by comparing the responses during the post-noise intervals.   Horizontal bars indicate the presentation time of the acoustic noise.

An example of the effect of acoustic noise duration on the fiber response during the post-noise interval is provided by Figure 10. While all three noise durations produce a decrement in responsiveness in the post noise interval, both the duration and the extent of this suppression are increased with increasing noise duration.

2.5   An explanation of the complex ECAP recovery pattern

We believe that a transient increase in firing synchrony in the post-noise interval (interval 5), combined with recovery from adaptation, gives rise to the complex, nonmonotonic, time course of ECAP recovery that has been detailed in previous progress reports (see QPR # 10, for example). During the post-noise recovery period, a brief period of ECAP amplitude enhancement is sometimes observed, followed by a period of depressed ECAP amplitude that eventually recovers.   This implies that the rates of "jitter recovery" and rate recovery are different. Our preliminary single-fiber data are consistent with that notion (this will be reported at a later date).

Based on the above observations, we might hypothesize that post-offset increases in fiber synchrony are due to the cessation and recovery of spontaneous activity. While spontaneous activity likely plays a role, it does not completely account for our observations. Figure 11 plots, as a function of spontaneous rate, the "electric+acoustic / electric" jitter ratios measured in interval 5 for our group of 41 fibers. Note that most jitter ratios are less than 1, indicating enhanced synchrony in the post-noise interval. However, note that jitter enhancements were observed for fibers with low or no spontaneous activity, something not predicted by our hypothesis. This result suggests that alteration of fiber temporal properties may also be due to previous neural activity. One way to examine this possibility would be to compare the post-offset fiber characteristics obtained with an acoustic masker and an electric masker.

To date, we have not been able to establish dependencies of fiber properties on the degree of jitter reduction in the post-offset interval. Figure 12 plots interval 5 jitter values for the combined "electric + acoustic" stimulus condition as a function of best frequency and fiber categories of spontaneous rate and electrophonic response. No strong dependency on best frequency is evident in this relatively small data set. Our future plan includes the collection of additional data to better address possible dependencies.
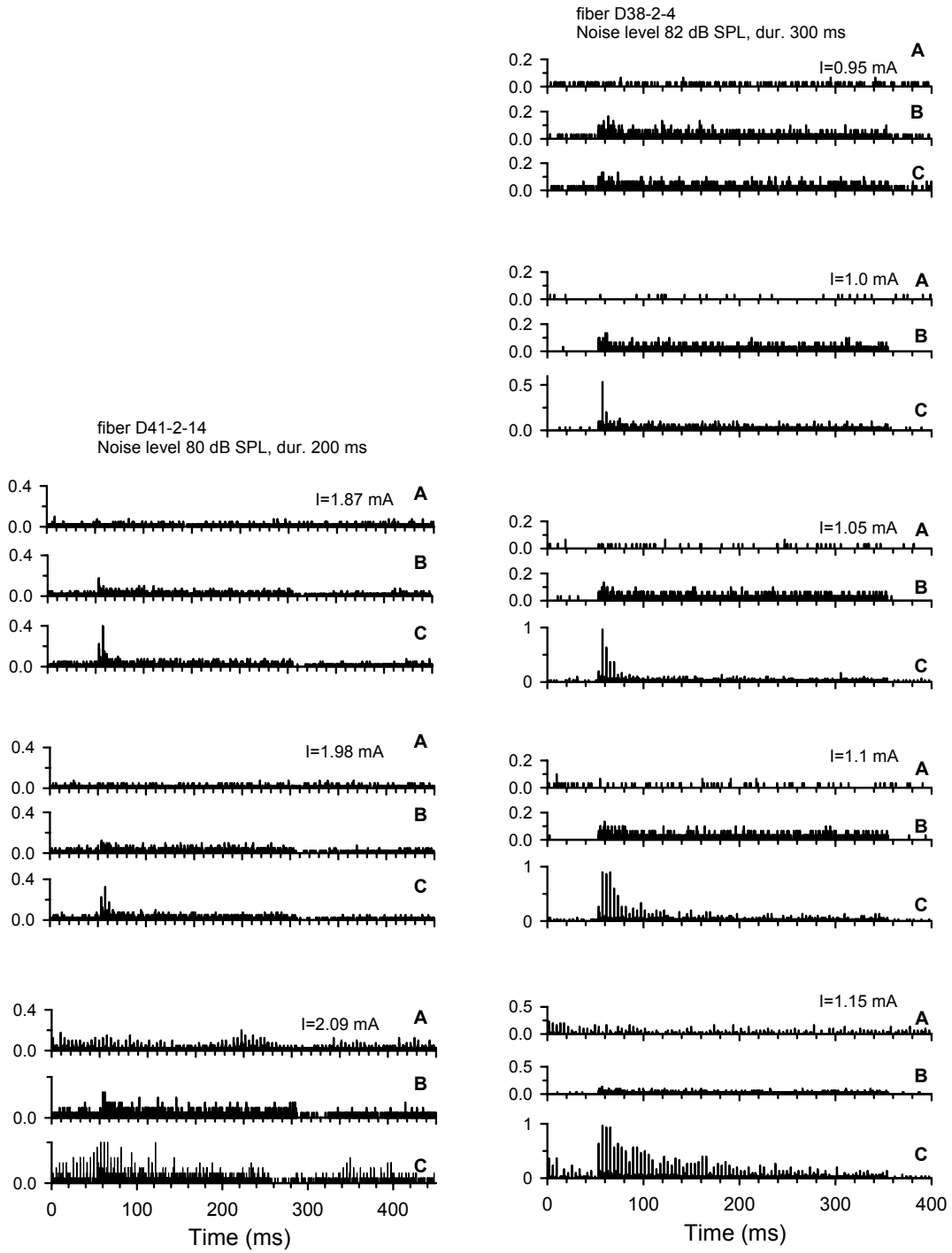
2.6   Enhanced electric responses

One of our original hypotheses suggested that some combinations of acoustic and electric stimuli could result in enhanced response, possibly through mechanisms at the hair cell or synapse level. To date, we have observed, in 5 fibers across as many subjects, increases in firing probability to the electric stimulus during presentation of the wideband acoustic noise stimulus. The degree and duration of these enhanced responses varies across fibers. Figure 13 provides examples of responses from two fibers. In both cases, however, the greatest enhancement of the electric response occurs shortly after onset of the acoustic
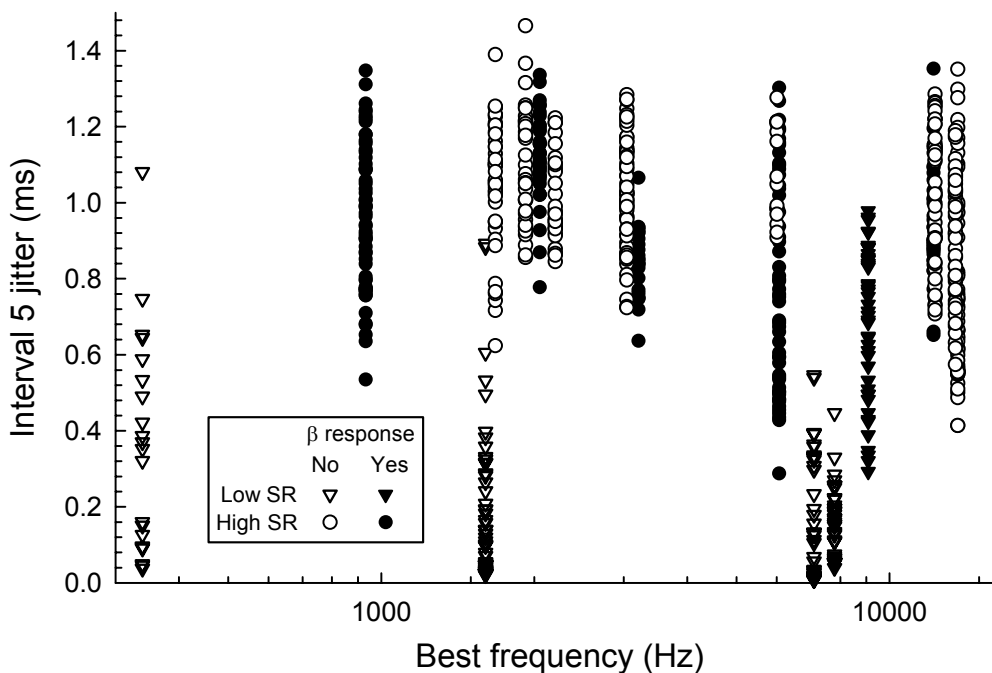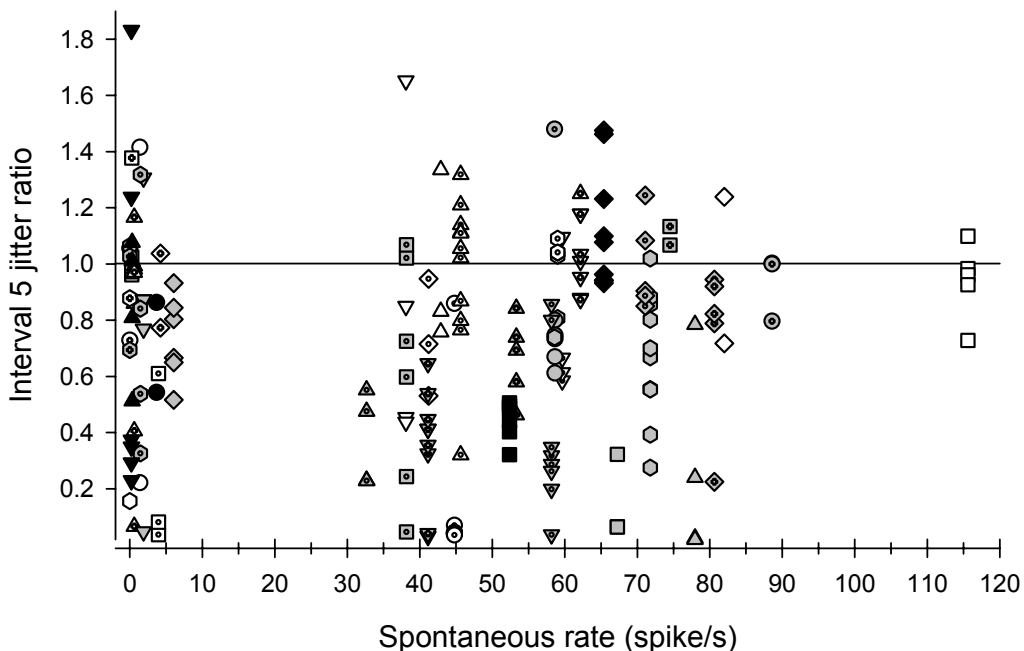
Figure 11 Ratio of jitter values ("Electric + Acoustic " / "Acoustic") following acoustic stimulation. Interval 5 jitter ratios are plotted as a function of spontaneous rate. Values less than one indicate reduced jitter in the post-noise interval relative to the jitter measures obtained in the electric-train alone condition. Each of the 41 fibers is assigned a different symbol in this plot. Multiple points per fiber reflect data obtained at multiple electric stimulus levels spanning the dynamic range of each fiber.

Figure 12 Absolute jitter values obtained in Interval 5 following the presentation of combined electric and acoustic stimulation. Data are plotted as a function of best frequency, with spontaneous rate and presence/absence of electrophonic responses coded by the symbol type, as shown.

Figure 13 Acoustically enhanced responses to electric pulse trains. PST histograms from two fibers are shown in the two columns. For each fiber, three panels (A, B. and C) correspond to the stimulus conditions of "electric alone", "acoustic alone", and "electric + acoustic", respectively.

stimulus. Note also that not only does the acoustic stimulus increase the synchronous firing probability in response to the electric train, but also decreases the electric threshold. Both of these alterations are consistent with a mechanism involving stochastic resonance. We have performed an analysis similar to that shown in Figure 12 to determine whether or not enhancements are related to single-fiber properties such as spontaneous rate or best frequency; the relatively small data set does not allow us to reach conclusions at this time. This issue will be pursued with additional data collection.

2.7   Discussion

This report demonstrates the feasibility of obtaining single-fiber responses to both electric and acoustic stimuli in cats using a minimally invasive intracochlear electrode. Previous efforts in obtaining electrically evoked responses while maintaining the responsiveness of the cochlea have indicated the vulnerability of the cochlear mechanism (as assessed by preservation of the electrophonic response) to placement of an intracochlear electrode. Our acoustic sensitivity data indicate some degree of sensitivity loss, although our overall incidence of electrophonic responses are comparable to that reported from cochlea stimulated only by an extracochlear electrode (van den Honert & Stypulkowski, 1984).

Single-fiber responses to our moderate rate electric pulse trains differ in several ways from those observed in deafened ears. Electrophonic responses, which were observed in about 20% of fibers, result in interval histograms with two prominent peaks (QPR 6, Figure 10) whose relative amplitudes are highly sensitive to stimulus level. Furthermore, the electrophonic response exhibited relatively fast adaptation to the pulse train. The temporal code of such fibers in response to electric trains would therefore be expected to be complex and may have significant perceptual consequences.

Another unique response pattern is the "build-up" response. Our initial estimate (to be examined in greater detail later) is that about 20% of the encountered fibers exhibit this pattern. As we noted, build-up responses have also been observed in the ECAP response using the same evoking pulse train. To date, we have seen this in three of six cat experiments. This response property could introduce an additional low-pass filter function to fiber responses. It is not clear what underlies this response; it has not been reported in the pulse train responses from deafened animals.

Finally, we note that the temporal uncertainty (jitter) of fibers is much greater – roughly an order of magnitude – than what is typically observed from deafened fibers (Miller et al., 1999). In our fiber sample collected to date, the degree of increased jitter correlates strongly with the level of spontaneous activity. Due to our windowing of spike activity used for jitter analysis, we believe it unlikely that the increased jitter is due mainly to the addition of a background level of random spikes which directly alter (increase) the estimates of timing variability. Rather, it seems more likely that this background activity

places fibers in varying states of partial refractoriness that give rise to increased temporal uncertainty.

The addition of acoustic stimulation during the presentation of electric pulses can result in a number of interactions. PST histograms indicate that the acoustic stimulus can desynchronize the neural response and effectively act as a simultaneous masker, reducing the responses to the electric pulses. Spike activity-related adaptation of the fiber can result in lowered responsiveness after cessation of the acoustic stimulus. These interactions are typical of the fibers we have encountered. However, a smaller number of fibers (perhaps 10%) exhibit enhanced electric responses during presentation of the acoustic stimulus. Moxon (1971) noted synergistic effects of electric and acoustic sinusoidal stimulation of single fibers. Due to the tuning and delay properties of fibers, one might not expect to observe large acoustically generated enhancements of ECAP responses, even though a significant number of fibers may exhibit enhanced responses.

2.8   References

Liberman M.C. (1978). Auditory nerve responses from cats raised in a low-noise chamber. J. Acoust. Soc. Am. 63, 442-55.

Liberman M.C., Kiang, N.Y. (1978). Acoustic trauma in cats. Cochlear pathology and auditory-nerve activity. Acta Otolaryngol. Suppl. 358, 1-63.

Liberman M.C. (1982). The cochlear frequency map for the cat: labeling auditory-nerve fibers of known characteristic frequency. J. Acoust. Soc. Am. 72, 1441-9.

Miller C.A., Abbas, P.J., Robinson, B.K., Rubinstein, J.T., Matsuoka, A.J. (1999). "Electrically evoked single-fiber action potentials from cat: responses to monopolar, monophasic stimulation." Hear. Res. 130, 197-218.

Moxon E.C. (1971). Neural and mechanical responses to electric stimulation of the cat's inner ear. Doctoral Dissertation. Massachusetts Institute of Technology.

Nourski K.V., Abbas P.J., Miller C.A., Robinson B.K., Jeng F.C. (2005). Effects of acoustic noise on the auditory nerve compound action potentials evoked by electric pulse trains. Hear. Res. 202:141-153.

Schroeder, M.R., Hall, J.L., 1974. Model for mechanical to neural transduction in the auditory receptor. J. Acoust. Soc. Am. 55: 1055-1060.

van den Honert, C., Stypulkowski, P.H. (1984) Physiological properties of the electrically stimulated auditory nerve. II. Single fiber recordings. Hear. Res. 14, 225-243.

3.   Addendum: 16-channel headstage design

This section briefly describes the 16-channel headstage amplifier used in our multi-unit recordings within the inferior colliculus. The basic circuit design of the headstage amplifiers was provided to us by Chris Ellinger of Kresge Hearing Research Institute of Ann Arbor, Michigan. An earlier version of this headstage was made for work conducted in a previous contract; an improved design (featuring improved cabling and shielding) was built for the current contract.

The headstage and its support components are shown in Figure 14. The **headstage board** consists of 16 non-inverting voltage followers. The electrical schematic diagram of this board is shown in Figure 15. Circuit board layouts are shown in Figures 16 and 17. A parts list for these boards is provided in Table 1. Note that he headstage board uses a double-sided copper clad board to reduce the board size.

A degree of protection of the amplifiers against static discharge through the thin-film electrode array is provided by 10 kΩ input resistors. The amplifiers are Texas Instruments TLC2274 low-power JFET-input operational amplifiers in surface-mount packages to main the low profile of the headstage board. The low-profile consideration can be critical when using a surgical microscopic to position and advance the thin-film array into tissue, particularly when the surgical assess or exposure to the target tissue is limited. These op-amps feature so-called "rail-to-rail" output capacity to maximize the output dynamic range. Outputs from the board are carried by a shielded cabled manufactured by ANS Portland (a division of Micro Helix , Inc.). This cable consists of fine (38 AWG) wires within a braided shield, Teflon wrap, and a urethane jacket that provides a relatively high degree of mechanical compliance, thus reducing the probability of mechanical tissue damage from forces transmitted through the cable. The wires of this cable are soldiered directly onto soldier pads on the headstage board. The cable is then "potted" to the board with an epoxy glue. This was done in lieu of a cannon-style connector to maintain the low profile of the headstage board.

This cable terminates in a small **interconnection board** by means of a "cannon" style connection. This small board provides additional mechanical isolation from the larger power-supply board and serves as a means of providing a more standard output cable to down-stream electronics. In our case, this interconnection board has two 8-pin female DIP plugs for interfacing with such external electronics. The headstage amplifiers are powered by two 9V batteries and d.c. regulators on the **power supply board**. This third board can be placed a greater distance from the animal preparation.

The headstage board is held in a small clamping fixture (roughly in the shape of a tuning fork) that provides a means of mating the headstage board to a micromanipulator through a 1 mm diameter shaft. This fixture clamps onto the sides of the DIP socket that holds the thin-film array, thus helping maintain alignment of the array with the axis of the micromanipulator.
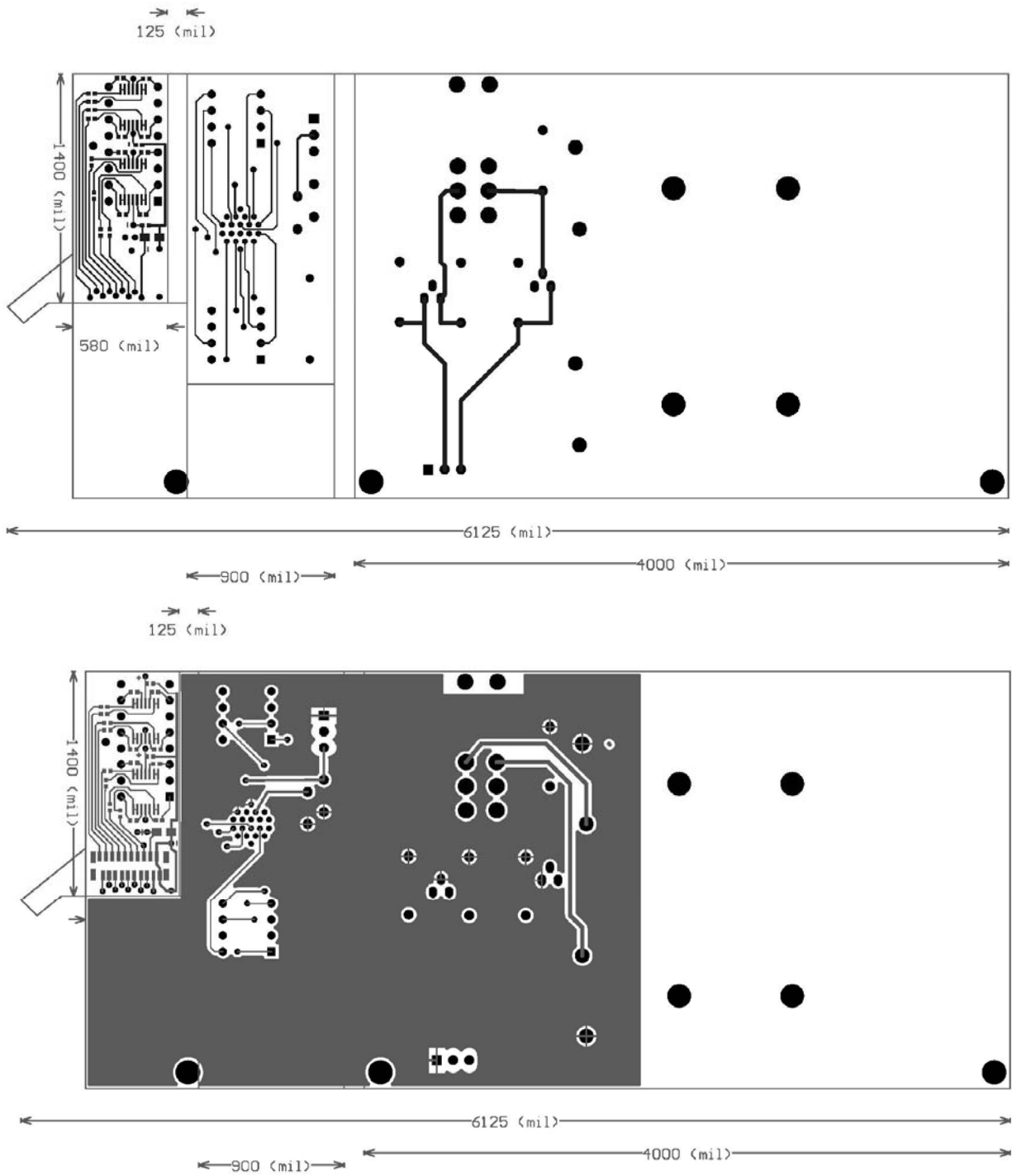
Additional information, including all original board layouts and artwork are available as a file package; please contact either Dr. Abbas or Dr. Miller.
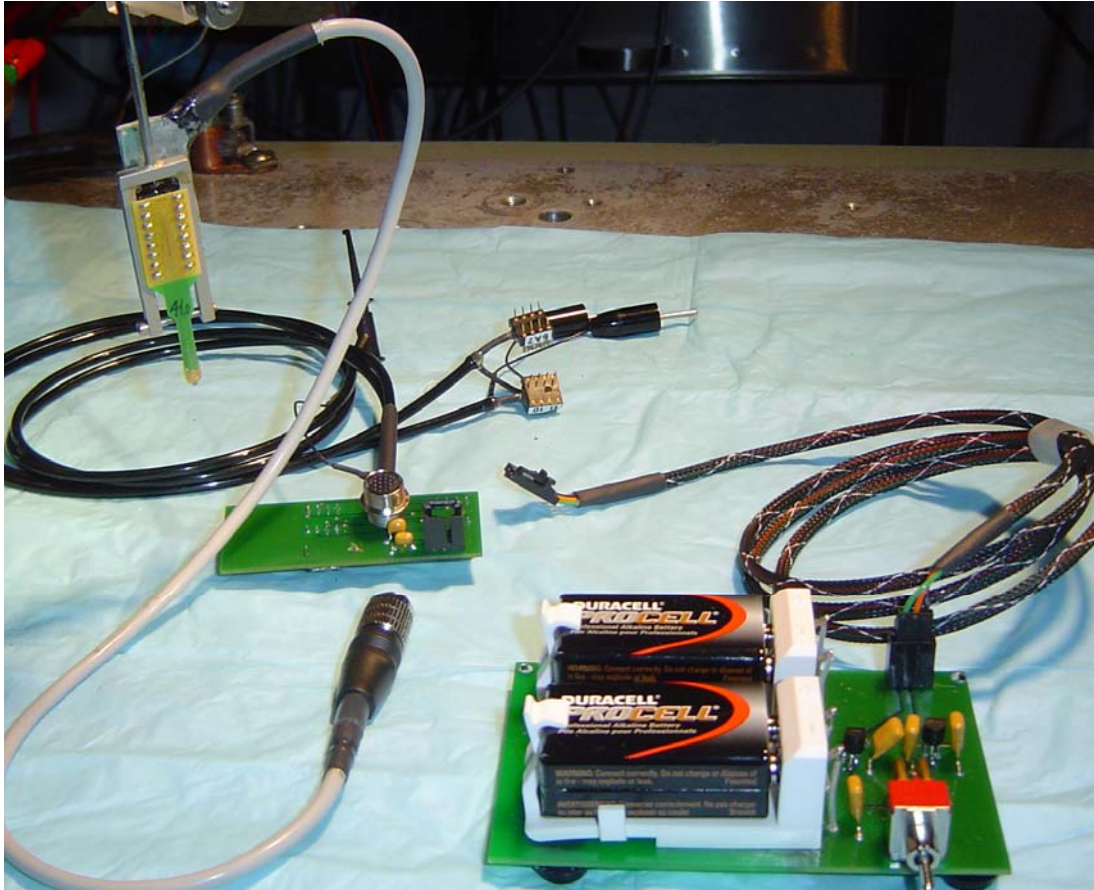

Figure 14 Photograph of the headstage system. A 16-channel thin-film electrode is shown mounted on the headstage board (upper left), which in turn is held by a U-shaped clamping fixture. A flexible shielded cable runs from the upper right corner of the headstage to an interconnection board (middle, left of center). This small board also provides a distribution point for the signal output cables (black cables in upper left) and the d.c. power supply (lower right).
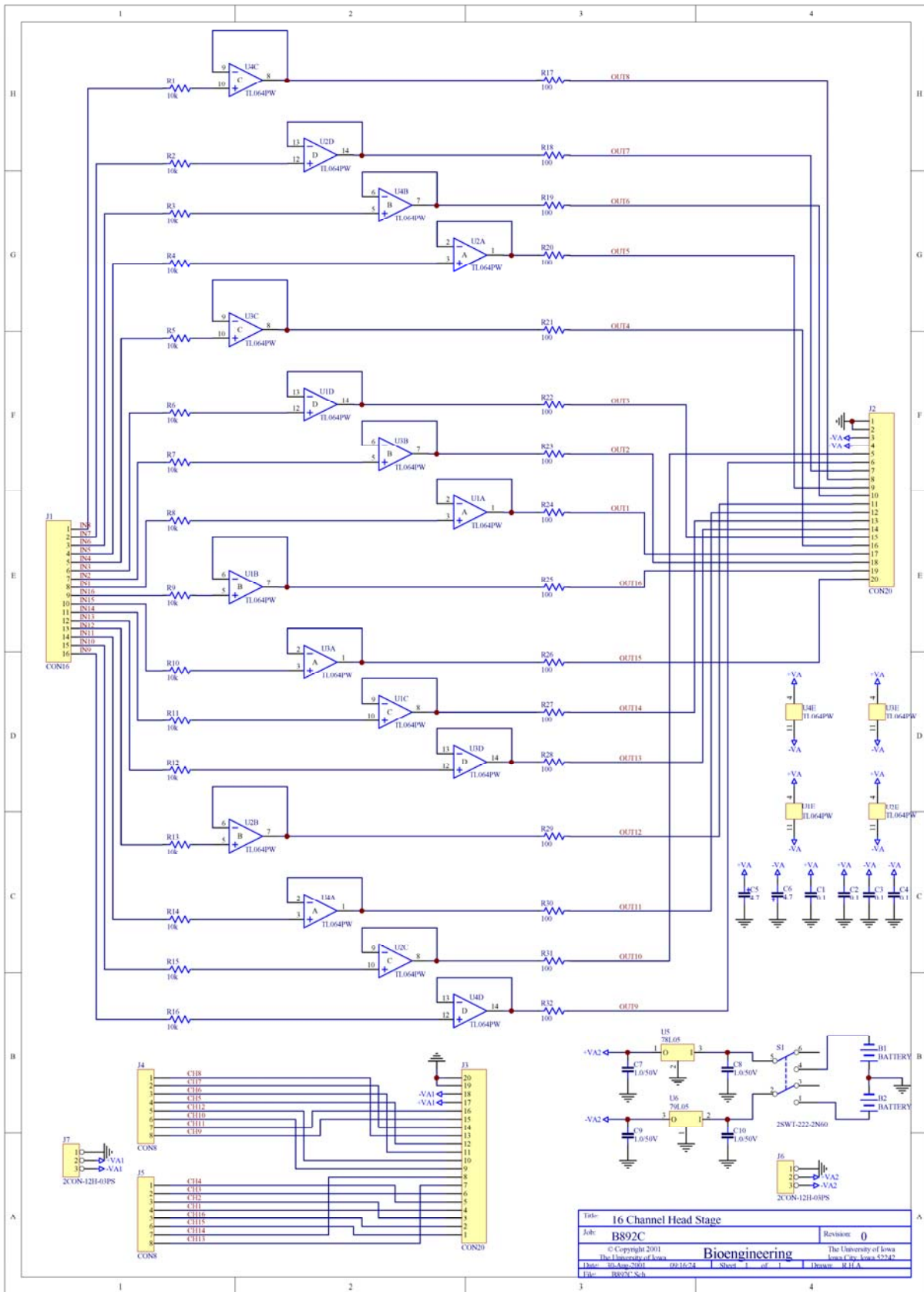
Figure 15   Schematic circuit diagrams of the three circuit boards. The diagram of the headstage board dominates this figure, while the interconnection board and power supply board are shown at the lower left and lower right, respectively.

125 (mil)

1400 (mil)

580 (mil)

6125 (mil)

4000 (mil)

900 (mil)

125 (mil)

1400 (mil)

6125 (mil)

4000 (mil)

900 (mil)

Figure 16 Circuit board mask patterns for (left to right), the headstage, the interconnection board, and the power supply board. A ground plane is preserved in the latter two boards. Figure 17 provides a more detailed view of the headstage masks.
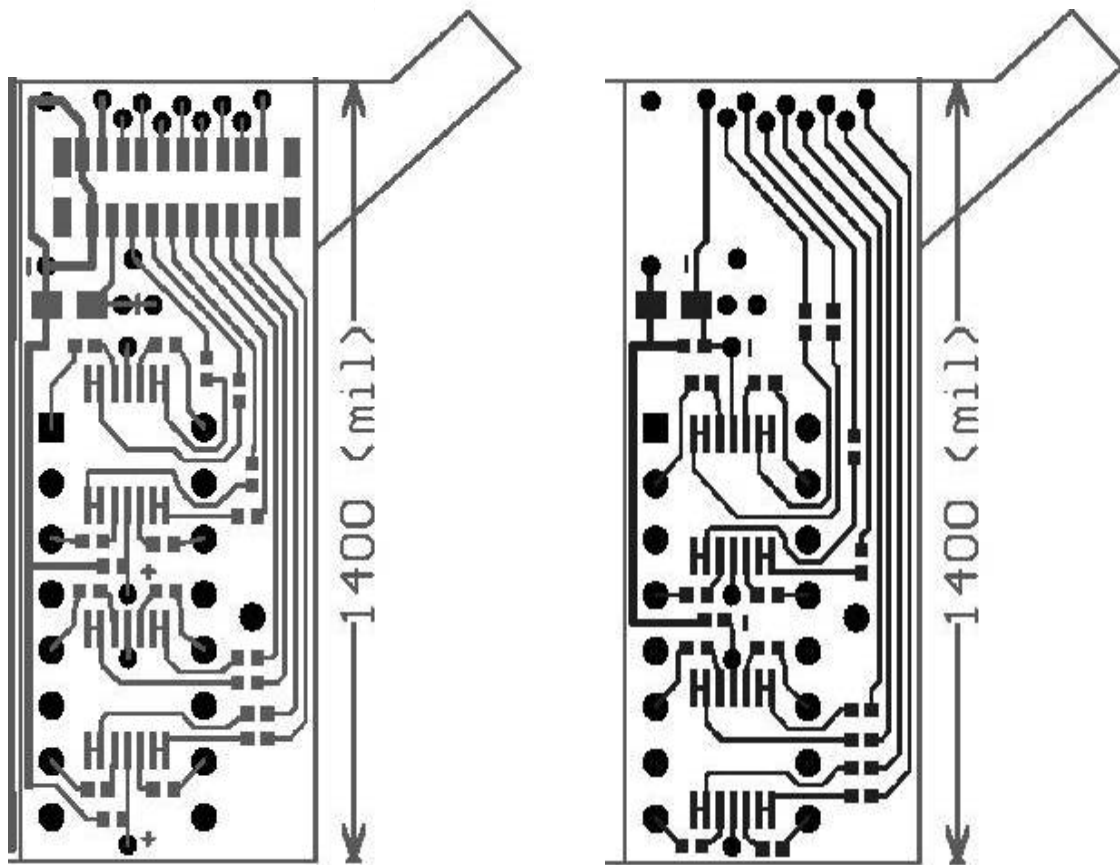
Figure 17   Layout of pads and runners on the headstage board. Four surface-mount op-amp footprints can be seen between the pads for the 16-pin DIP socket that accepts a 16-channel thin-film array. Pads for the output cable and strain-relief tab are seen at the top.

Designator	Part Type	Footprint	Description	Read-Only Field 1	Drawer	Digikey Part#	
B1	BATTERY	BAT-9V-PC	AA BATTERY	2BAT-HKY-1028			
B2	BATTERY	BAT-9V-PC	AA BATTERY	2BAT-HKY-1028			
C1	0.1	0402-1005	Capacitor	2CAP-$$$-$$$$		PCC1731CT	
C10	1.0/50V	CAP37	1.0/50V	2CAP-610-150C			
C2	0.1	0402-1005	Capacitor	2CAP-$$$-$$$$		PCC1731CT	
C3	0.1	0402-1005	Capacitor	2CAP-$$$-$$$$		PCC1731CT	
C4	0.1	0402-1005	Capacitor	2CAP-$$$-$$$$		PCC1731CT	
C5	4.7 10V	805	Polar Cap	2CAP-$$$-$$$$		P11340CT	
C6	4.7 10V	805	Polar Cap	2CAP-$$$-$$$$		P11340CT	
C7	1.0/50V	CAP37	1.0/50V	2CAP-610-150C			
C8	1.0/50V	CAP37	1.0/50V	2CAP-610-150C			
C9	1.0/50V	CAP37	1.0/50V	2CAP-610-150C			
J1	CON16	DIP16	Connector			AE9816-ND	
J2	CON20	FH12-20	Connector			HFL20CT-ND	
J3	CON20	FH12-20	Connector			HFL20CT-ND	
J4	CON8	DIP8	Connector				
J5	CON8	DIP8	Connector				
J6	2CON-12H-03PS	HEADER-PC-3	Header 3	2CON-12H-03PS	FD47		
J7	2CON-12H-03PS	HEADER-PC-3	Header 3	2CON-12H-03PS	FD47		
R1	10k	402	RC07	2RES-FCA-$$$$		P10KJCT-ND	50/200
R10	10k	402	RC07	2RES-FCA-$$$$		P10KJCT-ND	
R11	10k	402	RC07	2RES-FCA-$$$$		P10KJCT-ND	
R12	10k	402	RC07	2RES-FCA-$$$$		P10KJCT-ND	
R13	10k	402	RC07	2RES-FCA-$$$$		P10KJCT-ND	
R14	10k	402	RC07	2RES-FCA-$$$$		P10KJCT-ND	
R15	10k	402	RC07	2RES-FCA-$$$$		P10KJCT-ND	
R16	10k	402	RC07	2RES-FCA-$$$$		P10KJCT-ND	
R17	100	402	RC07	2RES-FCA-$$$$		P100JCT-ND	
R18	100	402	RC07	2RES-FCA-$$$$		P100JCT-ND	
R19	100	402	RC07	2RES-FCA-$$$$		P100JCT-ND	
R2	10k	402	RC07	2RES-FCA-$$$$		P10KJCT-ND	
R20	100	402	RC07	2RES-FCA-$$$$		P100JCT-ND	
R21	100	402	RC07	2RES-FCA-$$$$		P100JCT-ND	
R22	100	402	RC07	2RES-FCA-$$$$		P100JCT-ND	
R23	100	402	RC07	2RES-FCA-$$$$		P100JCT-ND	
R24	100	402	RC07	2RES-FCA-$$$$		P100JCT-ND	
R25	100	402	RC07	2RES-FCA-$$$$		P100JCT-ND	
R26	100	402	RC07	2RES-FCA-$$$$		P100JCT-ND	
R27	100	402	RC07	2RES-FCA-$$$$		P100JCT-ND	
R28	100	402	RC07	2RES-FCA-$$$$		P100JCT-ND	
R29	100	402	RC07	2RES-FCA-$$$$		P100JCT-ND	
R3	10k	402	RC07	2RES-FCA-$$$$		P10KJCT-ND	
R30	100	402	RC07	2RES-FCA-$$$$		P100JCT-ND	
R31	100	402	RC07	2RES-FCA-$$$$		P100JCT-ND	
R32	100	402	RC07	2RES-FCA-$$$$		P100JCT-ND	
R4	10k	402	RC07	2RES-FCA-$$$$		P10KJCT-ND	
R5	10k	402	RC07	2RES-FCA-$$$$		P10KJCT-ND	
R6	10k	402	RC07	2RES-FCA-$$$$		P10KJCT-ND	
R7	10k	402	RC07	2RES-FCA-$$$$		P10KJCT-ND	
R8	10k	402	RC07	2RES-FCA-$$$$		P10KJCT-ND	
R9	10k	402	RC07	2RES-FCA-$$$$		P10KJCT-ND	
S1	2SWT-222-2N60	DPDT-PC-AV2	DPDT-PC	2SWT-222-2N60			
U1	TLC2274	TSSO5X6-G14/X.3	Low-Power JFET-Input Op Amplifier			296-7124-6	
U2	TLC2274	TSSO5X6-G14/X.3	Low-Power JFET-Input Op Amplifier			296-7124-6	
U3	TLC2274	TSSO5X6-G14/X.3	Low-Power JFET-Input Op Amplifier			296-7124-6	
U4	TLC2274	TSSO5X6-G14/X.3	Low-Power JFET-Input Op Amplifier			296-7124-6	
U5	78L05	78LXX	5 Volt Regulator	2ICL-1FP-0501			
U6	79L05	78LXX	-5 Volt Regulator	2ICL-1FN-0501			

Table 1 Parts list and parts descriptions for circuit components of the16-channel headstage. Parts supplier was Digikey Corporation (http://www.digikey.com/).

4.   Plans for the next quarter

1. Complete off-line analysis of single-unit responses for all completed experiments.

2. Conduct additional single-fiber experiments to obtain more information on possible relationships among single fiber properties (best frequency, spontaneous rate, etc.) and the nature of acoustic-electric interactions.   Specifically, we wish to collect sufficient best-frequency information to address the question of whether or not the nature of the acoustic-electric interactions varies systematically with fiber-to-electrode distance. One such interaction of interest is the observed enhanced electric responses reported in this QPR.

3. Prepare manuscripts for publication detailing the single-fiber work. Two manuscripts are planned, one dealing with descriptions of the animal model, its capabilities, and the basic response properties of fibers stimulated by electric pulse trains and a second that examines electric/acoustic interactions as observed in single units, with an emphasis on interpreting the complex ECAP adaptation and recovery trends that have been reported previously.

4.   Continue to conduct experiments to determine if the acoustic-electric interactions observed at both the single-fiber and ECAP levels are specific to the two modes of stimulation or more generally due to the imposition of additional neural activity (nonspecific to the excitation mechanism). To this end, we will run parallel experiments, with one scheme that will replace the wide-band acoustic noise with an electric masking stimulus designed to evoke a comparable level of spike activity.

5. Present material related to this contract at the 2005 Conference on Implantable Auditory Prostheses. Three presentations will be given, covering ECAP, single-fiber, and IC studies.

6. Develop the aforementioned computational model such that it accepts both acoustic and electric stimulation and activity from either excitation route will feed back to refractory and adaptation processes. This model will assist in our interpretation of ECAP results.